UNIVERSITY OF CALIFORNIA
RIVERSIDE

Constructing a Broadband Spectroscopic Optical Coherence Tomography System and Improving Spectral Resolution With Phase Plate Theory

A Thesis submitted in partial satisfaction
of the requirements for the degree of

Master of Science

in

Bioengineering

by

Jason D. Qiu

December 2018

Thesis Committee:
Dr. B. Hyle Park, Chairperson
Dr. William H. Grover
Dr. Joshua Morgan

The Thesis of Jason D. Qiu is approved:

_____

_____

_____

Committee Chairperson

University of California, Riverside

ABSTRACT OF THE THESIS

Constructing a Broadband Spectroscopic Optical Coherence Tomography System and Improving Spectral Resolution With Phase Plate Theory

by

Jason D. Qiu

Master of Science, Graduate Program in Bioengineering
University of California, Riverside, December 2018
Dr. B. Hyle Park, Chairperson

Optical coherence tomography (OCT) is capable of high-resolution cross-sectional imaging of retinal tissue and is typically paired with near-infrared (NIR) wavelengths due to its ability to penetrate deeper into tissue when compared to visible wavelengths. This imaging modality has helped ophthalmologists diagnose and learn more about the structural changes found in retinal diseases. To help further the effectiveness and versatility of this imaging modality, broadband visible wavelengths were incorporated into the system to enable detection of spectroscopic signals. Wavelengths centered at 580 nm could provide valuable molecular information, such as oxygen levels in hemoglobin, that were not achievable with NIR wavelengths. The use of visible wavelengths and a novel spectroscopic analysis technique was demonstrated in a visible OCT system, which was then characterized and tested.

Table of Contents

List of Figures

Introduction

Introduction to OCT

Optical coherence tomography (OCT) is a high-resolution cross-sectional imaging technique that is frequently paired with near-infrared (NIR) wavelengths and used in clinical practice and research [4]. OCT uses the long wavelengths of NIR light to cross-sectionally image regions of tissue 1.5mm below the surface of the retina and is known for its noninvasiveness and high resolution (1-15μm) [1]. It has also enabled ophthalmologists to diagnose numerous eye conditions that were very difficult to detect in the past and has applications in a wide range of eye pathologies, such as age-related macular degeneration [2, 9], pigment epithelial detachments [2], and central branch retinal vein occlusions [2]. All materials have a unique spectroscopic signature that can be obtained through spectroscopy, which enables the detection of molecular changes found within a biological environment.

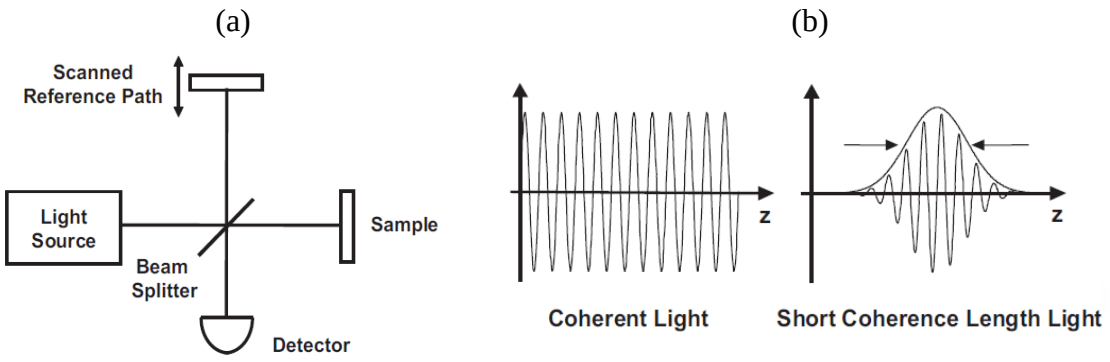

Figure 1 (a) A basic schematic of a Michelson interferometer. (b) An example of the difference between high coherence and low coherence light. [3]

Traditional OCT uses a Michelson interferometer as shown in Figure 1(a) and low-coherence light to generate an interference signal that contains information regarding the structures found in the sample [3]. Interference signals are prevalent when the optical distances of the sample arm and the reference arm differ by less than the coherence length of the light [13]. The axial resolution is dependent on the coherence length, so the broader the bandwidth or shorter the coherence length, the higher the axial resolution will be [4]. In OCT, a low coherence length is necessary in order to detect blood vessels and retinal layers, which are in the micrometer range. An example of the difference between high coherence and low coherence light is shown in Figure 1(b). It should be noted that the high coherence length light can be seen to constructively interfere with each other over long distances whereas the low coherence length light only constructively interferes with each other over short distances, which is termed as the light's coherence length. This coherence length is key to the functionality of the imaging modality OCT.

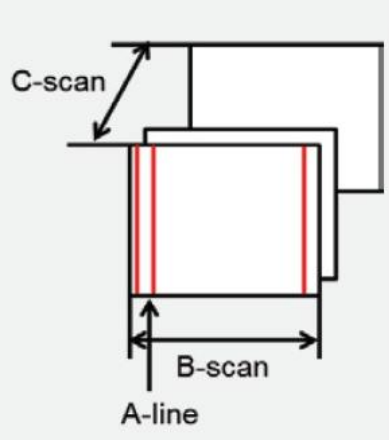

Figure 2 A schematic showing the A-line, B-scan, and C-scan that takes place when imaging with an OCT system [5].

As the incident beam of light travels through the sample of interest and is reflected off different reflectors at different depths, the frequencies found within the interference signal will change. A way to separate these different frequencies is with a Fourier transform, which will convert the interference signal from the time domain to the frequency domain effectively separating the frequencies into their own frequency-specific peaks [4]. These peaks each represent a different reflector found at a

different depth from the sample. By recording the intensity of the reflection at each depth, an intensity profile can be constructed. These intensity profiles are also called A-lines and contain information regarding the reflectivity of the structures found beneath the surface of the tissue. A single A-line can be obtained while the laser sits still on the sample. When the laser moves transversally across the sample, the system collects multiple A-lines in sequence. By combining these A-lines a B-scan can be formed. This B-scan is a two-dimensional data set that represents the cross-sectional tomographic image of the sample. Furthermore, by piecing together multiple B-scans, a C-scan is formed, which is a data set that represents a three-dimensional model of the imaging volume [5]. A schematic is shown in Figure 2 to graphically represent these different scans and how they fit together.

The imaging depth of the system is heavily reliant on the wavelengths of the source light, so NIR light, which has a longer wavelength than visible light, is used to penetrate the tissue 2-3 mm deep [10]. This typically covers all the layers of the human retina [6]. The downside of using NIR wavelengths in OCT is that it only allows the imaging system to detect structural information and does not provide useful spectral information, which would be helpful in disease diagnosis/studies because of the functional information it would provide [7]. Visible light is more sensitive at detecting chromophores like photopigment, melanin, and hemoglobin, which are all potential biomarkers for retinal diseases [7]. By using visible light, the system would be able to reveal important spectroscopic signatures, which can be used to detect oxygenated and deoxygenated hemoglobin in the capillary vessels of the retina, which has been found to be an early biomarker of early-stage diabetic retinopathy [8]. By combining OCT with visible

wavelengths, depth-resolved spectroscopic information should be distinguishable by the system.

Spectroscopic Analysis

To obtain spectroscopic information from the sample, the reflectance spectrum needs to be extracted from the interference pattern. This is done through MATLAB and can be accomplished by subtracting the frequencies from the interference signal using a short-time Fourier transform technique as described in Chong et al. [7]. This method will yield a reflectance spectrum, but there may still be some leftover modulation. This problem was addressed by placing a phase plate in the sample arm to create two images [12]. A phase plate is a piece of glass with a hole drilled through the center with a diameter smaller than the beam diameter. When light passes through the phase plate, it will cause the portion of the beam passing through the glass to have a longer optical path length than the portion of the beam passing through the hole due to the difference in the index of refraction. By increasing the number of images obtained to two, a more accurate spectroscopic reading can be determined by taking the average of both reflectance spectra. Figure 3 shows how the phase plate changes the optical path length of the beam.

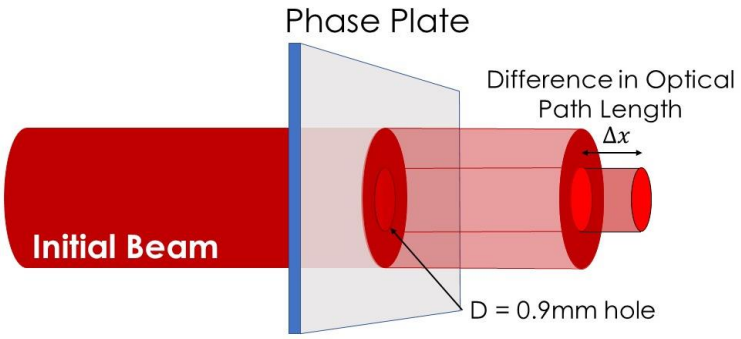

Figure 3 Simple schematic showing the phase plate altering part of the beam's optical path length when passing through the polycarbonate with a distance of Δx.

Materials and Methods

System Design

The hyperspectral OCT system used a broadband supercontinuum laser source with a wavelength range of 400nm – 2400nm. To isolate the wavelengths of interest, a dichroic mirror at a 45º angle to only permit a 560±50nm bandwidth was implemented. The collimated beam that left the laser source was then focused into a FiberPort collimator and then into a 90:10 fiber optic coupler, which sent 90% of the light into the reference arm and 10% of the light into the sample arm. This decision was made with the interest of conserving as much reflected sample arm light as possible. By sending 10% of the light into the sample arm, 90% of the light that is reflected will reach the spectrometer. The maximum power output from the supercontinuum source is 4.2W and since the retinal exposure limit according to ANSI is 0.24mW/cm, power would not be an issue. The light is then re-collimated into a reference arm and a sample arm. The reference arm consists of a moving stage with two mirrors mounted on top and one stationary mirror on the breadboard. The beam path would form a "U" shape and the path length of the reference arm could be adjusted using a micrometer, which would move the moving stage forward and backwards towards and away from the stationary mirror respectively. A focusing lens was placed right before the stationary mirror to increase the amount of light reflected back to the spectrometer. The sample arm includes a two-dimensional scanning galvanometer from Thorlabs and two achromatic lenses to ensure the beam is focused properly when scanning the sample. The incident beam power at the sample arm would be set below 0.24mW to satisfy the ANSI safety standards of combined optical power incident on the

retina. The light that is reflected off the sample is sent to the spectrometer. Both the sample arm and the reference arm will reflect light back through the 90:10 fiber optic coupler and into the custom-built spectrometer. The spectrometer consists of a collimator, a grating, an achromatic lens and a charge-coupled device (CCD) camera from Basler. The collimator focuses the light from the fiber into a collimated beam that is sent to the grating, which separates the light into an array of individual wavelengths horizontally. This spectrum of light is then focused by a lens into the CCD camera and subsequently processed by software. This system is characterized and used to take all the following data and images. A full model generated through SolidWorks is shown in Figure 4.

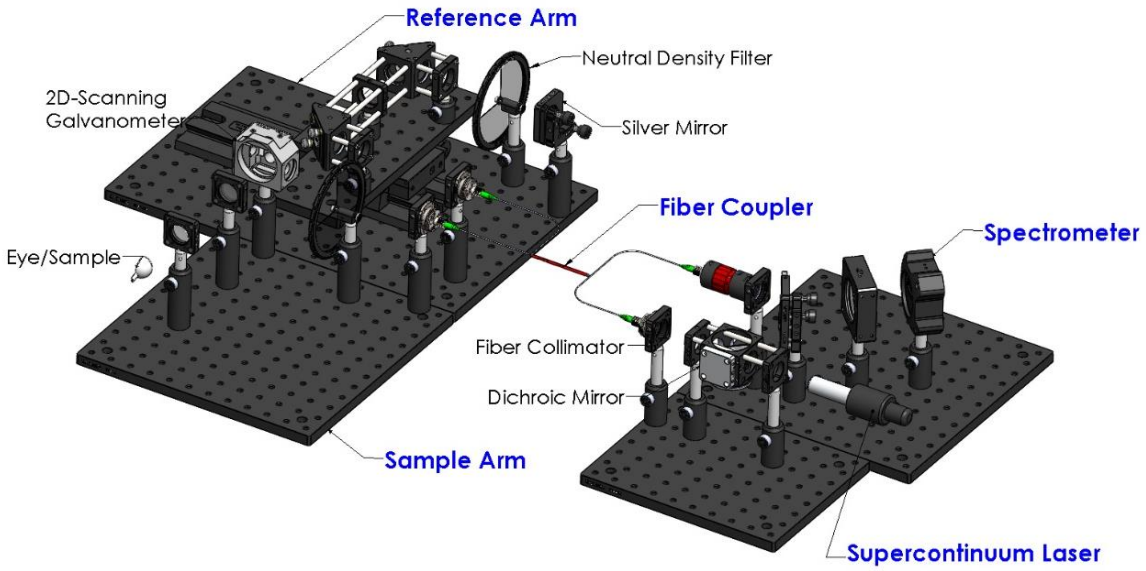

Figure 4 The supercontinuum laser emits a beam that passes through the dichroic mirror and isolates the wavelengths of interest by reflecting wavelengths less than 532nm and greater than 633nm to the beam dump. The light that does enter the fiber collimator is then split by the fiber coupler and sent in a 90:10 ratio to the reference and the sample arm respectively. The light that is sent to the sample arm is used to scan the sample and send any reflected information back to the spectrometer. The reference arm light needs to match the sample arm's optical path length to within the coherence length of the light source in order to obtain an interference pattern after the spectrometer picks up both signals from the reference and the sample arm. The light that travels to the spectrometer is split into individual wavelengths by a diffraction grating and focused into a CCD camera, which is then sent to the computer for processing.

System Characterization

To characterize the spectroscopic OCT system, the axial resolution, lateral resolution, sensitivity, signal roll off, and spectral resolution were determined. The axial resolution was determined by placing a silver-coated mirror at the end of the sample arm and taking a recording. MATLAB was then used to find the FWHM of the point spread function (PSF) obtained from the image of the silver mirror. The width of the PSF can be calculated by first determining how many μm each pixel represents by taking the physical depth of the imaging range and dividing it by the total number of pixels. In this case the physical depth is 4mm and the total number of data points in the imaging range is 24,560. Therefore, each data point is equivalent to 0.163μm, which when multiplied by the total number of pixels in the imaging range gives the FWHM. The theoretical axial resolution can be calculated with Eq. 1, where Δz is the axial resolution, λ is the center wavelength, and $\Delta\lambda$ is the bandwidth.

$$\Delta z = \frac{2ln2}{\pi}\frac{\lambda^2}{\Delta\lambda} \quad (1)$$

When determining the lateral resolution, a 1951 US Air Force target from Edmund Optics shown in Figure 5 was used. The air force target was placed at the end of the sample arm and an *enface* scan was taken of the target. An *enface* scan means instead of imaging in a cross-sectional manner, imaging is done in a top-down forward-facing manner. The patterns shown on the air force target are sized according to the resolution standard. The smallest pattern that can still be distinguished as "black-white-black-white-black" will help determine the lateral resolution limit of the system. The lateral resolution is dependent on

Figure 5 A USAF 1951 air force target used to determine the lateral resolution of the spectroscopic OCT system.

the center wavelength, the focal length of the scanning lens, and the beam diameter. The system was centered at 582nm with a focal length of 50mm and a beam spot of 2.5mm in diameter. This information can be used to calculate the theoretical lateral resolution using Eq. 2 where λ is the center wavelength, *f* is the focal length of the scanning lens, and *d* is the diameter of the collimated beam.

$$\textbf{\textit{Theoretical Lateral Resolution}} = \frac{4\lambda}{\pi}\frac{f}{d} \qquad \textbf{(2)}$$

To determine the sensitivity of the system, a silver-coated mirror was placed at the end of the sample arm with a step neutral density filter (NDF) in the way of the beam of the source arm. The lights were turned off to make sure the noise floor was accurately measured. The NDF was then moved step by step up the optical density scale until the peak that represented the silver mirror was as low as it could be without it disappearing completely. A recording was taken of that image and MATLAB was used to determine the peak height of the mirror. The amount of power blocked by the NDF was then added to the peak height to obtain the system's sensitivity in decibels (dB).

The signal roll-off of the system was determined by placing a silver-coated mirror at the end of the sample arm and moving the image using the reference arm down the imaging screen away from the focus. The total distance of the imaging area is 4mm and by watching how the signal decreases as it moves down the imaging area, the signal roll-off of the system can be determined.

The spectral resolution was determined by taking the bandwidth of the system and dividing it by the number of pixels in the CCD line scan camera. To determine the bandwidth of the system two wavelength filters were used. One filter that only lets 532nm±5nm wavelengths pass through and one at 633nm±5nm. The positions of the wavelengths that were allowed through are shown in Figure 6. An image of a mirror was recorded with each of the filters in the source arm and used to determine what wavelengths were entering the line scan camera. Then by dividing the bandwidth by the number of pixels in the line scan camera (2048) the number of wavelengths per pixel is obtained.

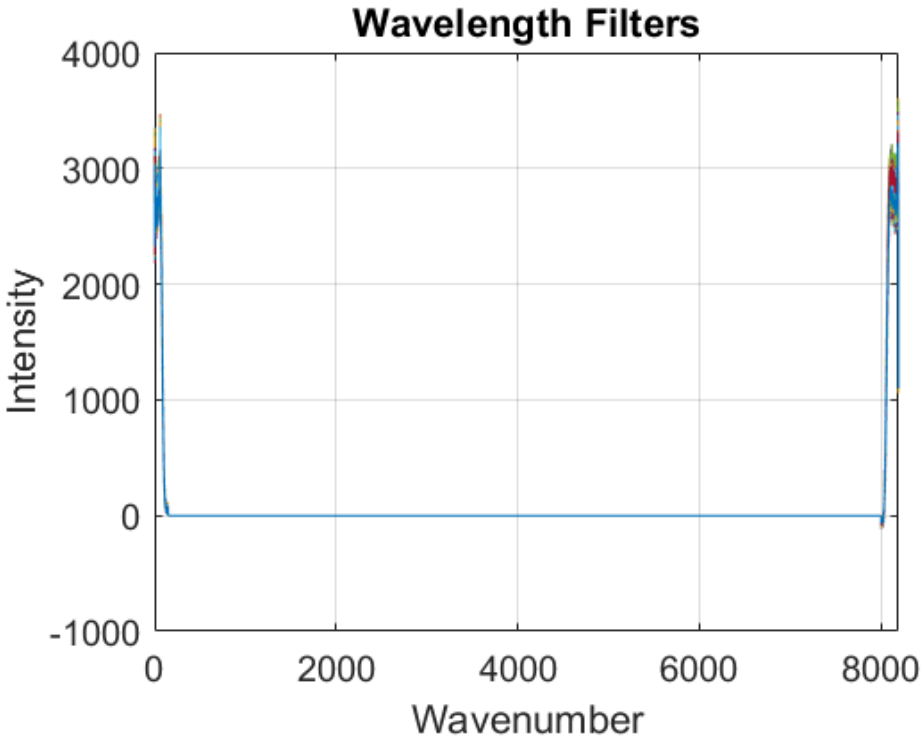

Figure 6 A MATLAB generated plot depicting what wavelengths each filter lets into the camera. There are two different peaks seen at the right and left edges of the plot, which are the 533nm filter and the 633nm filter respectively. The bandwidth of the system can now be determined with these measurements.

Phase Plate

Figure 7 The phase plate mounted into a 5-axis kinematic mount. The 0.5mm diameter hole at the center of the phase plate will create a difference in the optical path length and help improve spectroscopic resolution. The micrometers will assist in properly aligning this optical component at the center of the beam path.

The phase plate was created using clear PC-300^{TM} Polycarbonate from SciCron Technologies, LLC. It was 4.67mm thick with a 0.5mm diameter hole drilled through it. The edges of the polycarbonate slab were shaped into a 1-inch diameter circle in order to fit into the 5-axis kinematic mount. Figure 7 shows the phase plate mounted into the translational mount. The optical path length can be calculated by using Eq. 3 where D is the optical path length, *i* is the index of refraction of the media, and *d* is the distance the beam of light travels through the media. The optical path length between the light that travels through the polycarbonate and the light that travels through the air will differ because of the difference of the index of refraction between the polycarbonate and air. This difference in optical path length will result in a ~1.8mm distance between the two images to ensure that there is no overlap when recording data. The phase plate was then placed in the beam path in the sample arm before the galvanometer and aligned. Eq. 3 is shown below where D is the optical path length, *i* is the index of refraction of the media, and *d* is the distance the beam travels through the media:

$$D = id \quad (3)$$

Image Processing

The CCD line scan camera receives varying intensities of light for each wavelength and is dependent on the light that is reflected off the sample at the end of the sample arm. The interference pattern that is obtained from the reflected light is read into the acquisition program, which can then process these patterns using a "Fast Fourier Transform" (FFT) function to shift the interference signal from the time domain into the frequency domain to see what depth the reflectors in the sample arm are at. This information can help generate a depth profile or A-line of the sample, which can be combined with sequential A-lines to form a B-scan. A B-scan is a two-dimensional data set representing a cross-sectional image of the sample. Furthermore, by combining multiple B-scans a three-dimensional C-scan can be generated.

Spectroscopic Processing

Obtaining spectroscopic information from the visible OCT system is done through MATLAB processing. A recording of a mirror at the end of the sample arm was taken and the modulation was subtracted from the interference pattern to obtain the spectroscopic information. This process can be repeated with both images formed by the phase plate and by averaging the two spectra, a more accurate reading with less leftover modulation can be obtained.

Results & Discussion

System Characterization

Axial Resolution

After recording an image of the silver-coated mirror MATLAB was used to determine the axial resolution, which turned out to be 5.87µm. The peak obtained from the mirror is shown in Figure 8 and the vertical lines represent the FWHM of the point spread function. A FWHM of about 36 data points wide was observed and by multiplying the distance of each pixel (determined by dividing the imaging range by the number of data points) by the number of data points, the axial resolution can be obtained. The axial resolution of the visible OCT system should be better when compared to NIR light sources because of the resolution's dependence on the center wavelength as was shown in Eq. 1, which will improve the system's ability to resolve depth [4].

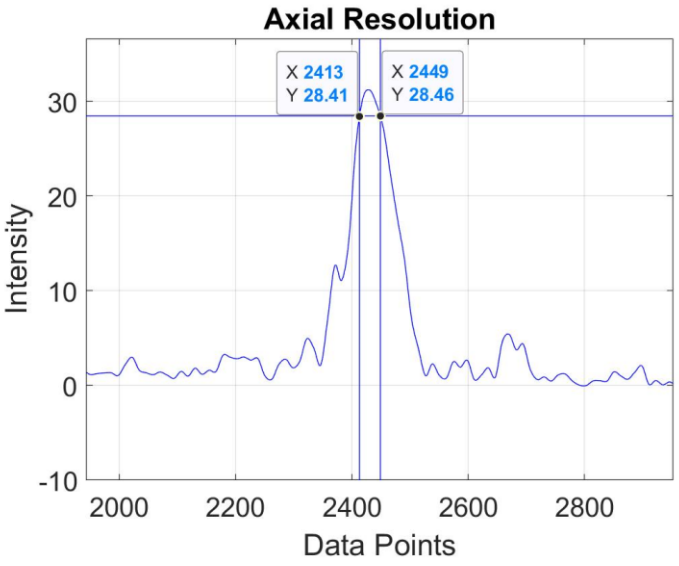

Figure 8 An image of the mirror and vertical indicator lines at the FWHM of the point spread function. This distance of about 36 data points which when multiplied by the 0.163µm/data point gives an axial resolution of 5.87µm.

Lateral Resolution

The lateral resolution of the system was determined to be 12.4µm using the USAF 1951 air force target. Figure 9 shows the *en face* image taken of groups 6 and 7 of the air force target using the system. Group 6 Element 1 was the

smallest pattern that was clearly distinguishable as “black-white-black white-black” without overlapping.

The theoretical lateral resolution was also calculated to be 14.8μm using Eq. 4:

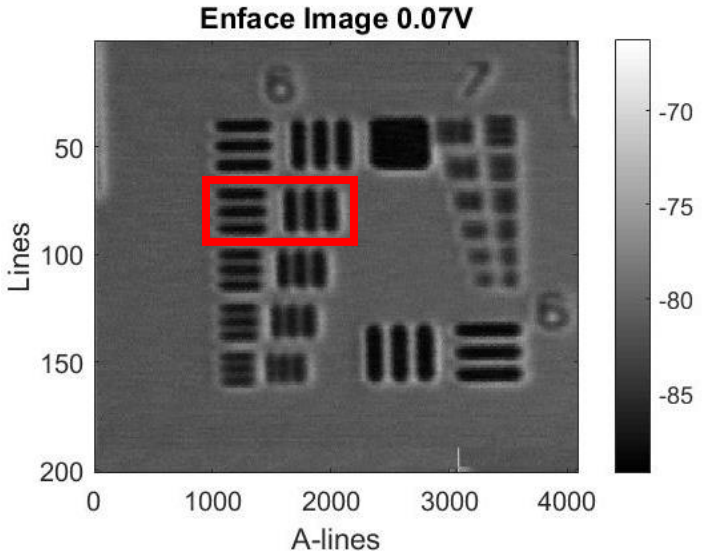

Figure 9 *En face* image of the USAF air force target taken with the spectroscopic OCT system. Groups 6 and 7 are shown in the image with Group 6 Element 3 being the smallest pattern that can still be distinguished which is indicated by the red box.

$$\boldsymbol{Theoretical = \frac{4\lambda}{\pi}\frac{f}{d} = \frac{4 \times 582nm}{\pi}\frac{50mm}{2.5mm} = 14.8\mu m} \qquad \textbf{(4)}$$

Where *f* is the focal length of the objective, λ is the center wavelength, and *d* is the beam diameter. The actual lateral resolution is a bit better than the theoretical, but variation in the parameters of the system could account for this. Again, with a smaller center wavelength, the resolution improves when compared to traditional NIR wavelengths.

System Sensitivity

The sensitivity of the system was determined to be 93.94dB as shown in Figure 10. The peak height was around 33.94dB and the neutral density filter was at an optical density level of 3.0 in the beam path, so it blocks 30dB in each direction as the beam needs to travel through the NDF twice totaling to 60 dB of light blocked. Adding the amount of light blocked to the peak height totals to a system sensitivity of 93.94dB with 0.24mW at the incident beam, which is adequate for imaging biological samples [11].

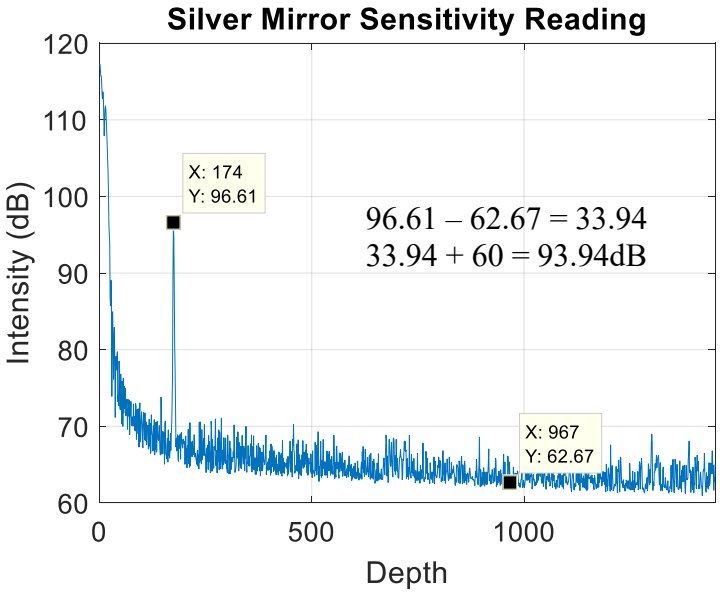

Figure 10 The intensity profile of the silver-coated mirror shows a peak at pixel 174 with a peak height of 33.94dB. The system was being blocked by a 3OD NDF and by adding the peak height to the amount of light blocked (60dB) a sensitivity of 93.94dB is obtained.

System Sensitivity Roll-Off

The system's sensitivity roll-off was shown to be ~5-6 dB per millimeter in Figure 11. The signal was able to travel all the way to the end of the axial imaging range, which is a total distance of 4mm. This is comparable to other visible OCT systems indicating that the system is properly aligned [4]. So, when using the system to image tissue, a signal drop of more than 12dB at around 2mm deep into the sample can be expected.

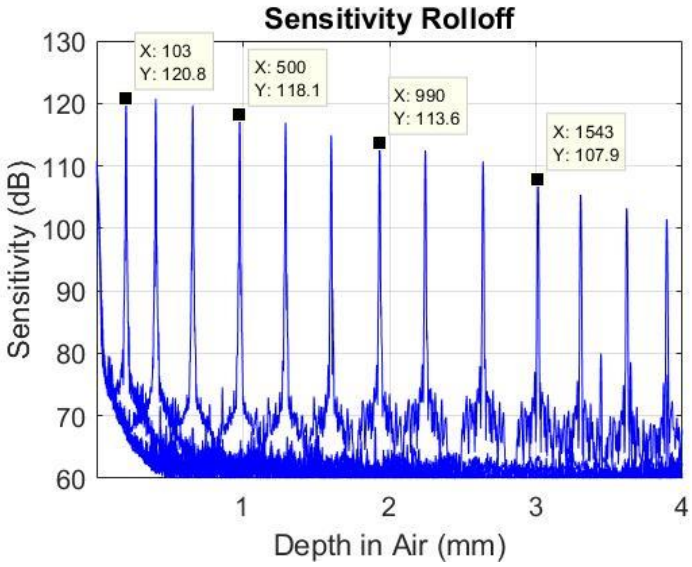

Figure 11 The sensitivity roll-off is shown using a silver mirror and incrementally decreasing the optical path length of the reference arm so that the image travels through the axial imaging range going from left to right.

Spectral Resolution

The system's spectral resolution is calculated by taking the bandwidth of the light and dividing it by the number of pixels in the CCD line scan camera. The bandwidth of the light that is sent into the sample is 101nm and the number of pixels in the camera is 4096. Therefore, the spectral resolution is 0.02nm/pixel. Figure 12 depicts the technique used to characterize the spectral resolution of the system.

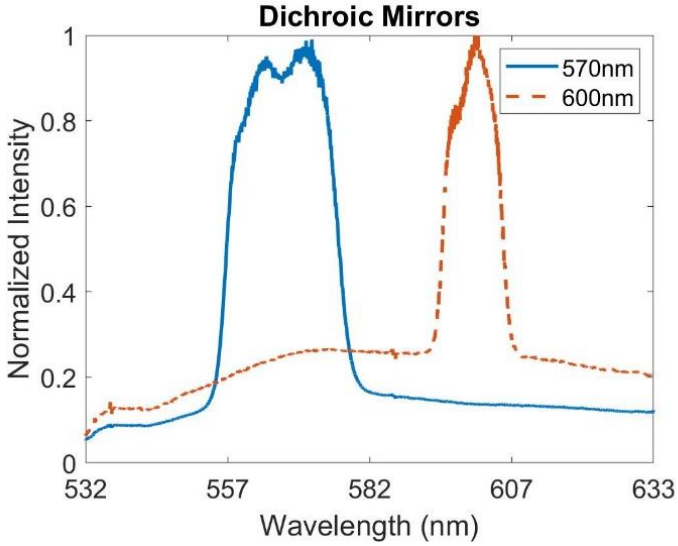

Figure 12 Spectra obtained by placing two of several different dichroic mirrors in the beam path that only permits 570±10nm and 600±10nm, which are the blue solid line and the orange dotted line respectively. By comparing the change or shift in spectra when changing the mirrors, a better understanding of how finely the system can differentiate between two different wavelengths can be established.

Phase Plate

The phase plate that was fabricated is shown in Figure 13(A). The hole drilled in the polycarbonate was 0.5mm in diameter and was decided after testing holes of various sizes that it was ideal for having relatively equal intensities for both images that it formed. Figure 13(B) shows the two peaks indicated by the info-markers. The third peak at 3mm is artifact and is just a result of internal reflection within the reference arm.

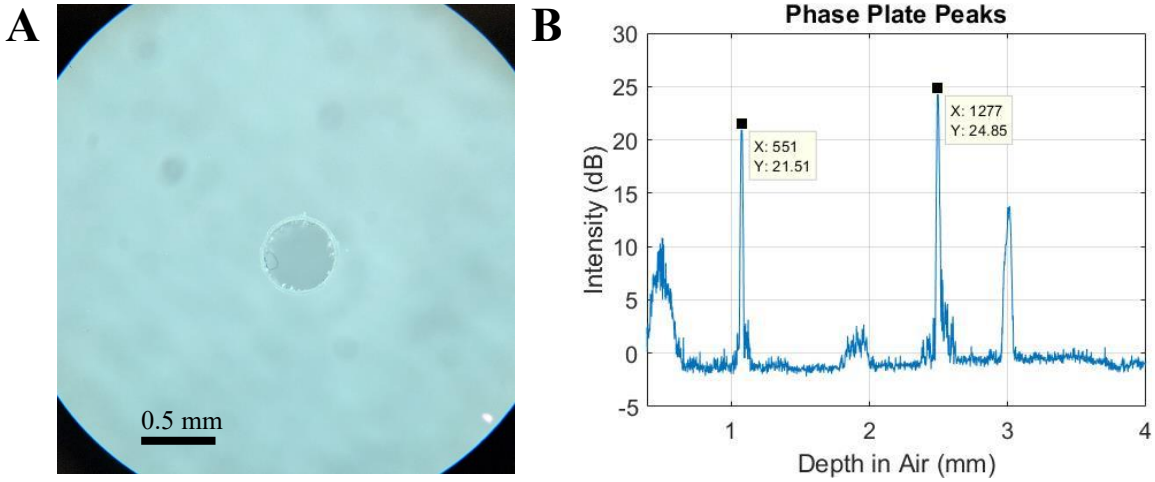

Figure 13 (A) The hole that was drilled into the polycarbonate slab and used to generate two different peaks by creating a difference in optical path length. (B) Two peaks are shown as a result of placing the phase plate in the beam path.

Image Processing

Figure 14(A) shows the raw spectrum obtained from the CCD camera of a silver-coated mirror. There is an underlying curve and an interference signal overlaying that curve. The interference signal (or modulation) contains the depth information at that A-line and can be isolated via an FFT in MATLAB. Once an FFT is performed on the raw spectrum, the signal is displayed in the frequency domain, which is also called an intensity profile.

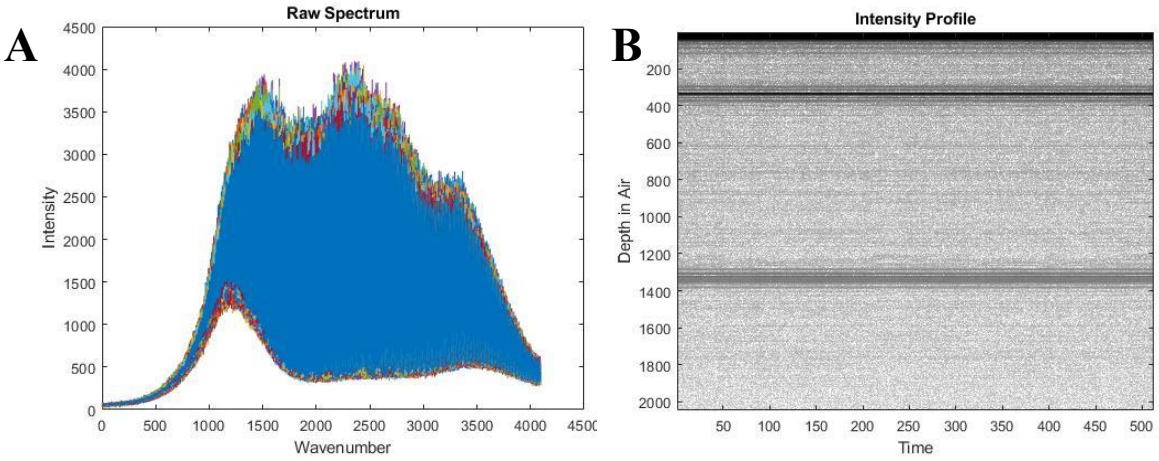

Figure 14 (A) Screenshot of the raw spectrum obtained from the CCD line scan camera, which contains spectral information as well as depth information. (B) Once the depth information is extracted, an intensity profile shown in 13(B) can be obtained.

This shows where the reflectors are located in the imaging range based off the frequency information obtained from taking the FFT. Figure 14(B) shows what the intensity profile looks like in grayscale. The dark horizontal line shown in the imaging space is where the silver-coated mirror is located.

Figure 14(B) only shows the intensity profile of just one A-line, which when combined with multiple A-lines, can form a cross-sectional intensity profile. Figure 15 shows the image obtained by scanning across a finger and by taking all the A-lines and combining them. This forms a cross-sectional data set of a finger.

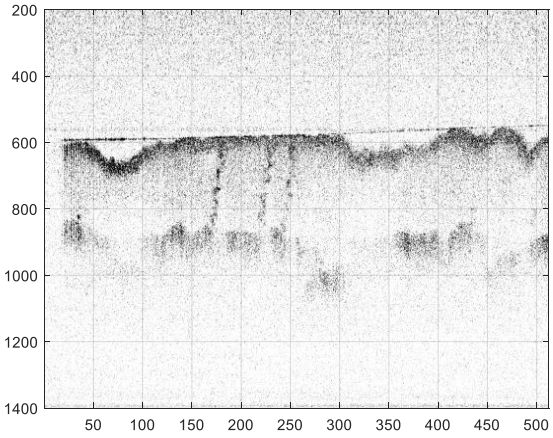

Figure 15 A cross-sectional data set of a finger. A lot of reflection from the initial surface is seen as well as some weaker reflection coming from sub-surface structures.

Conclusion

Traditional optical coherence tomography techniques utilize NIR wavelengths, which are ideal for structural imaging and deep tissue penetration. Unfortunately, NIR light is not ideal for identifying chromophores found in biological tissue, whereas visible light is. Introducing broadband visible light sources into OCT imaging expands the type of information this imaging modality can collect and can further the study and diagnosis of diseases.

The drawbacks of using visible light in OCT were more scattering in biological tissue resulting in a decreased imaging depth and chromatic aberration. On the other hand, advantages of visible wavelengths included spectroscopic data as well as improved axial and lateral resolution. There is a wealth of information coming from the visible wavelengths used as opposed to just the NIR wavelengths used in traditional OCT. The detection of retinal morphology is still very critical and will always be a staple in eye care. But the introduction of spectroscopic OCT generates questions about known diseases and their pathologies, which pushes researchers to study not just the structure, but also the molecular function found within the spectroscopic data.

References

[1] Huang, D., Swanson, E. A., Lin, C. P., Schuman, J. S., Stinson, W. G., Chang, W., ... & Fujimoto, J. G. (1991). Optical coherence tomography. *Science (New York, NY)*, *254*(5035), 1178.

[2] Ţălu, Simona-Delia. 2013. "Optical Coherence Tomography in the Diagnosis and Monitoring of Retinal Diseases." *International Scholarly Research Notices* 2013 (February). Hindawi. https://doi.org/10.1155/2013/910641.

[3] Drexler, W., & Fujimoto, J. G. (2015). Optical coherence tomography: technology and applications. Springer.

[4] Shu, Xiao, Lisa Beckmann, and Hao Zhang. 2017. "Visible-Light Optical Coherence Tomography: A Review." *Journal of Biomedical Optics* 22 (12): 1–14.

[5] Reif, Roberto, and Ruikang K. Wang. 2012. "Label-Free Imaging of Blood Vessel Morphology with Capillary Resolution Using Optical Microangiography." *Quantitative Imaging in Medicine and Surgery* 2 (3): 207–12.

[6] Fujimoto, James G. 2003. "Optical Coherence Tomography for Ultrahigh Resolution in Vivo Imaging." *Nature Biotechnology* 21 (11): 1361–67.

[7] Chong, Shau Poh, Marcel Bernucci, Harsha Radhakrishnan, and Vivek J. Srinivasan. 2017. "Structural and Functional Human Retinal Imaging with a Fiber-Based Visible Light OCT Ophthalmoscope." *Biomedical Optics Express* 8 (1): 323–37.

[8] Blair, Norman P., Justin Wanek, Anthony E. Felder, Charlotte E. Joslin, Jacob K. Kresovich, Jennifer I. Lim, Felix Y. Chau, Yannek Leiderman, and Mahnaz Shahidi. 2017. "Retinal Oximetry and Vessel Diameter Measurements With a Commercially Available Scanning Laser Ophthalmoscope in Diabetic Retinopathy." *Investigative Ophthalmology & Visual Science* 58 (12): 5556–63.

[9] Reif, Roberto, and Ruikang K. Wang. 2012. "Label-Free Imaging of Blood Vessel Morphology with Capillary Resolution Using Optical Microangiography." *Quantitative Imaging in Medicine and Surgery* 2 (3): 207–12.

[10] Fujimoto, J. G., C. Pitris, S. A. Boppart, and M. E. Brezinski. 2000. "Optical Coherence Tomography: An Emerging Technology for Biomedical Imaging and Optical Biopsy." *Neoplasia* 2 (1-2): 9–25.

[11] Shau Poh Chong, Conrad W. Merkle, Dylan F. Cooke, Tingwei Zhang, Harsha Radhakrishnan, Leah Krubitzer, and Vivek J. Srinivasan, "Noninvasive, in vivo imaging of subcortical mouse brain regions with 1.7 μm optical coherence tomography," Opt. Lett. 40, 4911-4914 (2015)

[12] Jianhua Mo, Mattijs de Groot, and Johannes F. de Boer, "Focus-extension by depth-encoded synthetic aperture in Optical Coherence Tomography," Opt. Express 21, 10048-10061 (2013)

[13] J. M. Schmitt, "Optical coherence tomography (OCT): a review," in IEEE Journal of Selected Topics in Quantum Electronics, vol. 5, no. 4, pp. 1205-1215, July-Aug. 1999.doi: 10.1109/2944.796348